

# Linearizing the Observed Power Spectrum

Clay C. Smith,<sup>1</sup>★ Anatoly Klypin,<sup>1</sup>★ Michael A. K. Gross,<sup>2</sup>★ Joel R. Primack,<sup>2</sup>★ and Jon Holtzman<sup>1</sup>★

<sup>1</sup>Department of Astronomy, New Mexico State University, Las Cruces, NM 88003 USA

<sup>2</sup>Physics Department, University of California, Santa Cruz, CA 95064 USA

15 September 2018

## ABSTRACT

Semi-analytic treatment of the power spectrum with the approximation of constant linear bias provides a way to compare cosmological models to a large amount of data, as Peacock & Dodds (1994, 1996; hereafter PD94 and PD96, respectively) have shown. By applying the appropriate corrections to the observational power spectrum it is possible to recover the underlying linear power spectrum for any given cosmological model. Using extensive N-body simulations we carefully test and calibrate all important corrections. To demonstrate that the method is applicable to a wide range of cosmological models, we tested the standard  $\Omega = 1$  cold dark matter (CDM) model,  $\Omega < 1$  models that include a cosmological constant ( $\Lambda$ CDM), and  $\Omega = 1$  models with a mixture of cold and hot dark matter (CHDM), both with one massive neutrino and two equal mass neutrinos. The  $\Lambda$ CDM and CHDM models are normalized to *COBE* and to cluster abundances. Our tests indicate that the improved linear–nonlinear mapping recently suggested by PD96 for treating CDM-type power spectra works well for a wide range of scale-dependent power spectra. However, we find that the recovery of the linear power spectrum from observations following PD94, which is often used to test cosmological models, can be misleading because the corrections are model-dependent. A model should not be judged based on the linear spectrum recovered by that procedure, but must be compared with the recovered spectrum for that particular model. When we apply the proper corrections for a given model to the observational power spectrum, we find that no model in our test group recovers the linear power spectrum well for the bias values suggested by PD94 between Abell, radio, optical, and *IRAS* catalogs:  $b_A : b_R : b_O : b_I = 4.5 : 1.9 : 1.3 : 1.0$ , with  $b_I = 1.0$ . The recovered linear  $\Lambda$ CDM and CHDM power spectra were systematically below their respective linear power spectra using  $b_I = 1.0$ . When we allow  $b_I$  to vary (keeping the same bias ratios) we find that: (i) CHDM models give very good fits to observations if optically-selected galaxies are slightly biased ( $b_O \sim 1.1$ ). (ii) Most  $\Lambda$ CDM models give worse but acceptable fits if blue galaxies are considerably antibiased ( $0.6 \lesssim b_O \lesssim 0.9$ ) and fail if optical galaxies are biased. (iii) There is a universal shape of the recovered linear power spectrum of all  $\Lambda$ CDM models over their entire range of explored wavenumbers,  $0.01 \lesssim k \lesssim 0.6 h \text{ Mpc}^{-1}$ . For a given bias, recovered linear power spectra of CDM and CHDM models are nearly the same as that of  $\Lambda$ CDM in the region  $0.01 \lesssim k \lesssim 0.2 h \text{ Mpc}^{-1}$  but diverge from this spectrum at higher  $k$ . We tabulate the recovered linear spectra, and also the initial linear spectra, for all the models considered.

**Key words:** cosmology: theory – large-scale structure of Universe

## 1 INTRODUCTION

\* E-mail:  
aklypin@nmsu.edu (AK); gross@physics.ucsc.edu (MAKG);  
joel@ucolick.org (JRP); holtz@nmsu.edu (JH)

The power spectrum of density fluctuations  $P(k)$  is a powerful tool for investigating the large-scale structure of the Universe. It is a useful statistical test of the distribution of matter from the scales of galaxy groups through scales

larger than superclusters, and it discriminates between cosmological models (see, for example, Liddle et al. 1996ab; Ma 1996; Klypin, Primack, & Holtzman 1996, hereafter KPH96). However, there are several obstacles that must be overcome to relate the observed nonlinear power spectrum to theoretical linear power spectra. Because observations typically give estimates for luminous objects in redshift space while theoretical models describe dark matter in real space, the differences between luminous and dark matter must be taken into account before a direct comparison between data and theory can be made.

Since the radial positions of galaxies are determined from their observed recession velocities, any peculiar motions (from either linear or nonlinear growth of fluctuations) will distort their placement. Kaiser (1987) estimated the effect for long waves in the linear regime and included a scale-independent bias. This correction applies to the region  $k \lesssim 0.1 h \text{ Mpc}^{-1}$  but not to smaller scales which are in the nonlinear regime. To treat this region, Peacock (1992) used a simplified model to estimate the effect of random motions in collapsed objects on the observed power spectrum. Peacock & Dodds (1994, hereafter PD94) combined the two separate effects, along with the overall bias level, into a single convenient expression that is claimed to remove these effects from the nonlinear power spectrum.

Additional nonlinear effects must be accounted for as well. Theory provides a linear power spectrum for a cosmological model, but the spectrum of the real universe has undergone significant modification because of nonlinear evolution. Numerical simulations are useful for estimating the nonlinear power spectrum but are time consuming and computationally expensive. A more practical approach would be to devise a general method for analytically constructing the nonlinear power spectrum from the linear power spectrum. This would allow any model to be evaluated quickly and open the possibility of directly removing nonlinear effects from a real power spectrum. Throughout this paper we will refer to the method of recovering the linear spectrum from the raw observational spectrum by applying a set of corrections as the ‘linearization’ procedure. We will refer to the inverse of linearization, the method of predicting the nonlinear spectrum of galaxies starting from the linear dark matter spectrum, as the ‘nonlinearization’ procedure.

Several advances in developing linearization methods have been made in the last few years. By considering the collapse of spherical structures and the nonlinear evolution in the limit of stable clustering, Hamilton et al. (1991, hereafter HKLM) devised an analytical method for relating the linear correlation function on a linear scale to the nonlinear correlations on a smaller, nonlinear scale. PD94 extended this method to power spectra, allowed for open models and models with a cosmological constant, and provided a fitting formula optimized by a series of numerical simulations. This semi-analytical method worked reasonably well for scale-free power-law spectra, but failed for models with spectral indices  $n \lesssim -2$  including scale-dependent spectra like those of CDM models that tend to  $n \sim -3$  on the smallest scales. Like HKLM, PD94 expected that their series of corrections would be nearly model-independent and could be applied to observational power spectra to arrive at the underlying linear power spectrum of the Universe. Not long after, however, Jain, Mo, & White (1995) found that there is indeed

a significant dependence on the model through the spectral index  $n$  of the linear power spectrum and suggested that an ‘effective index’ be used to treat curving spectra like those of CDM or CHDM models. This prompted Peacock & Dodds (1996, hereafter PD96) to revise their earlier fitting formula to include dependence on  $n$ , and propose that  $n$  should vary with scale to treat curving spectra.

In this paper we adopt the analytical form of the redshift corrections of PD94 and the improved linear-nonlinear semi-analytical approximation of PD96, although we find it necessary to modify both of these slightly. We have extensively tested each step of the procedure using numerical simulations of unbiased dark matter in CDM,  $\Lambda$ CDM, and CHDM models. We find that the redshift corrections of PD94 are close to those that we determine from our simulations, although they are improved when we use the appropriate 1D velocity dispersions for each model instead of universally applying  $300 \text{ km s}^{-1}$ . We also demonstrate that our modification of the linear-nonlinear mapping of PD96 works very well for the cosmologies that we examine; CDM,  $\Lambda$ CDM, and CHDM models are all well fit.

Having found that the method can handle a variety of models, we applied it to a compilation of observational power spectra (APM, APM/Stromlo, CfA-2, QDOT, and radio galaxies, and Abell clusters). Our intended goal is to demonstrate that the linear power spectrum can be recovered from concrete catalogs of objects in redshift space or real space for a number of interesting cosmological models and then use this technique to determine which model best fits the observed power spectrum. Because the corrections are model-dependent (mostly through the shape of the linear power spectrum), no simple scheme can reproduce the underlying linear spectrum without detailed information about the model. This dictates that we must select well-defined models and try to reconstruct their linear power spectra using the appropriate corrections *for each model*. For this reason, the widely used power spectrum of PD94 is of limited utility, since no model was specified. Several papers have used this power spectrum as a means for testing cosmological models (e.g., Liddle et al. 1996ab; Ma 1996; Coble, Dodelson, & Frieman 1996). We assert that this is incorrect and can lead to incorrect conclusions. The only measure of success of a particular model in this context is its ability to reconstruct the linear power spectrum from the *model-dependent* linearization of the observational power spectrum.

We have followed PD94 in assuming that the bias is linear and constant, and in our choice of observational data, but we have propagated the errors somewhat differently. We also considered a form of scale-dependent bias for one model. We have used the bias ratios of PD94, but we allowed the reference level  $b_1$  to float and by adjusting the overall bias level we optimized the fit of the linearization to the linear power spectrum for each model. We find that the linearization of the observational power spectra according to the  $\Lambda$ CDM family of models can all be described by the same shape and amplitude for a given bias level. In contrast, linearizations of CHDM models do not have a common form. Moreover, it appears that there is no universal linearized power spectrum since CDM,  $\Lambda$ CDM, and CHDM linearizations are all easily distinguishable. In addition, we arrive at the conclusion that optically selected galaxies must be an-tibiased ( $b_O \simeq 0.6 - 0.9$ ) if they are to be compatible with

the  $\Lambda$ CDM family of models. The estimates of the optical biases of different models from POTENT analyses by Hudson et al. (1995) seem to indicate that a small amount of anisotropies is acceptable for some models, though Peacock (1996) would disagree. Optical galaxies in CHDM models must be slightly biased ( $b_0 \simeq 1.1$ ), which would probably tend to favor CHDM models.

This paper is organized as follows. The details of our simulations are described in §2. §3 lists the various power spectra in the observational data set. In §4 we review the semi-analytic method in depth. We discuss the tests of the method and its application to our simulations in §5. The linearized observational power spectra for all the models that we consider are presented in §6. Our results are summarized in §7. Appendix A gives theoretical power spectra for all the models considered.

## 2 NUMERICAL SIMULATIONS

In order to fully test our semi-analytical approximations, we performed an array of numerical simulations of several different cosmological models. All simulations were performed using standard Particle-Mesh (PM) codes (Hockney & Eastwood 1981; Kates, Kotok, & Klypin 1991; Smith 1995; Klypin, Nolthenius, & Primack 1997; Gross et al. 1997). Table 1 lists the models and gives their defining parameters. We used the ‘standard’ cold dark matter model (SCDM) with bias  $b = \sigma_8^{-1} = 1.5$ , four different flat  $\Lambda$ CDM models, and two  $\Omega = 1$  CHDM models. The CHDM<sub>0.7</sub> model has one neutrino species and the CHDM<sub>0.8</sub> model has two equally massive neutrino species. Except for SCDM, all our simulations started from *COBE*-normalized Gaussian initial conditions.

Table 2 shows the box sizes, resolutions and number of realizations for each model. Multiple box sizes and realizations were simulated for many models in order to reduce the impact of two effects which can change estimates of the nonlinear power spectrum as calculated from simulations. (1) Cosmic variance can cause significant fluctuation of the power spectrum on large scales due to poor counting statistics. Averaging the power spectra of several smaller realizations together reduces this effect significantly. (2) Small box sizes ( $L \lesssim 100 h^{-1}$  Mpc) have the effect of reducing the power in the nonlinear region of the power spectrum by as much as 50 per cent, leading to an underestimation of the scale at which nonlinear effects begin to appear. This is due to the fact that long waves (which are coupled to shorter waves) cannot be present in the box. Boxes with  $L \gtrsim 200 h^{-1}$  Mpc are better for constructing accurate power spectra of the quasi-nonlinear region because the first several bins at small  $k$  then lie in the truly linear regime. By using boxes with  $L = 300 h^{-1}$  Mpc for most of the models discussed in this paper, we address both problems.

For CDM-type spectra like those that we examine in this paper, (with or without a cosmological constant, but not including CHDM), the primordial spectrum is modified by physical processes that can be expressed in a scale-dependent transfer function,  $T(k)$ . Since the shape of the CDM spectrum does not change much after the epoch of equality, it is a function of  $k$  only. The power spectrum of

the tilted CDM-type models considered here can thus be approximated as

$$P(k) = A k^n T^2(k) \frac{g^2(\Omega(t))}{g^2(\Omega_0)} \quad (1)$$

where  $g(\Omega, \Omega_\Lambda)$  is the growth rate of fluctuations used to specify the power spectrum at different epochs and  $T(k)$  is the transfer function. We use the approximation of Carroll, Press, & Turner (1992) (cf. also Lahav et al. 1991),

$$g(\Omega, \Omega_\Lambda) = \frac{5}{2} \Omega \left[ \Omega^{4/7} - \Omega_\Lambda + \left(1 + \frac{\Omega}{2}\right) \left(1 + \frac{\Omega_\Lambda}{70}\right) \right]^{-1}, \quad (2)$$

where  $\Omega_\Lambda \equiv \Lambda/(3H_0^2)$ . The SCDM transfer function that we used was the commonly used approximation of Bardeen et al. (1986, BBKS), which has the form

$$T(q) = \frac{\ln(1 + 2.34q)}{2.34q} \times [1 + 3.89q + (16.1q)^2 + (5.46q)^3 + (6.71q)^4]^{-1/4} \quad (3)$$

where  $q = k/(h\Gamma)$  and  $\Gamma$  is the ‘shape parameter’ defined by Sugiyama (1995) (but cf. Hu & Sugiyama 1996 for improved spectra).

$$\Gamma = \Omega_0 h \exp(-\Omega_b - \Omega_b/\Omega_0). \quad (4)$$

Here,  $\Omega_b$  is the contribution of baryonic matter to the cosmological density. However, we only used the BBKS transfer function with  $\Gamma = 0.5$  for SCDM. For our other simulations, the transfer functions of the  $\Lambda$ CDM and CHDM models we used were calculated from a full Boltzmann treatment updating that in Holtzman (1989); fitting formulas are given in Appendix A. For CHDM models, the different time-dependent growth rates of the cold and hot species means that the shape of the power spectrum changes over time. Incorporating the growth rates into the transfer function gives a general form of the CHDM power spectrum,

$$P_{\text{CHDM}}(k) = A k^n T^2(k, \Omega(t)). \quad (5)$$

The CHDM transfer functions were essentially those of Klypin et al. (1993) and Primack et al. (1995); cf. Appendix A.

In all, we have three classes of dark matter models with a total of seven distinct models. Our sampling covers a wide range of power spectra with shallow (SCDM), medium ( $\Lambda$ CDM), and steep (CHDM) spectral indices on small scales, which allows us to test our method thoroughly.

## 3 OBSERVATIONAL DATA

The observational power spectra to which we will apply our linearization methods consist of six independent data sets and two cross correlations between data sets, as assembled by PD94. Included in the sample are catalogs of optical clusters, radio galaxies, optical galaxies, and galaxies from the *IRAS* catalog. Each is briefly described below.

One set of a real-space power spectrum is included, the APM power spectrum (Baugh & Efstathiou 1993). It is arrived at by deprojecting the angular clustering of individual galaxies from the APM survey. Because it only deals with angular positions, it directly yields the real-space power spectrum without the need to correct for redshift-space effects. Of the full data set, we choose to examine only points in

**Table 1.** Summary of model parameters

Model	$\Omega_0^a$	$\Omega_\Lambda^b$	$\Omega_{c+b}^c$	$\Omega_b^d$	$h^e$	$n^f$	$\sigma_8^g$	$Q^h$	$\Gamma^i$
SCDM	1.0	0.0	1.0	0.00	0.5	1.00	0.67	8.49	0.50
$\Lambda\text{CDM}_{0.3}$	0.3	0.7	0.3	0.026	0.7	1.00	1.10	22.0	0.20
$\Lambda\text{CDM}_{0.4}$	0.4	0.6	0.4	0.035	0.6	0.975	1.00	21.8	0.23
$\text{TACDM}_{0.4}$	0.4	0.6	0.4	0.035	0.6	0.90	0.873	24.7	0.23
$\Lambda\text{CDM}_{0.5}$	0.5	0.5	0.5	0.035	0.6	1.00	0.818	13.93	0.29
$\text{CHDM}_{0.7}$	1.0	0.0	0.7	0.10	0.5	1.00	0.676	17.0	0.39
$\text{CHDM}_{0.8}$	1.0	0.0	0.8	0.10	0.5	1.00	0.719	18.44	0.34

<sup>a</sup> Matter density parameter.<sup>b</sup> Cosmological constant density parameter  $\Omega_\Lambda \equiv \Lambda/(3H_0^2)$ .<sup>c</sup> Cold dark matter density parameter + baryon matter density parameter.<sup>d</sup> Baryonic matter density parameter.<sup>e</sup> The Hubble parameter specified as  $h \equiv H_0/(100 \text{ km s}^{-1} \text{ Mpc}^{-1})$ .<sup>f</sup> Index of the power spectrum on large scales.<sup>g</sup> Linear mass fluctuation amplitude  $(\Delta M/M)_{\text{rms}}$  smoothed with a top-hat filter of radius  $8 h^{-1} \text{ Mpc}$ .<sup>h</sup> Quadrupole of CMBR anisotropy  $Q_{\text{RMS-ps}}$ .<sup>i</sup> Sugiyama (1995) shape parameter  $\Gamma = \Omega_0 h \exp(-\Omega_b - \Omega_b/\Omega_0)$ . The actual spectral shape of the CHDM models is steeper for large  $k$  than the  $\Lambda\text{CDM}$  models, contrary to the impression that the high values of  $\Gamma$  for these models might give. Note that the value of the modified shape parameter  $\Gamma = 0.5(0.95\sigma_8/3.5\sigma_{25})^{3.33}$  introduced in Borgani et al. (1997) is nearly identical to the Sugiyama shape parameter for all but the two CHDM models, for which it would be 0.16 and 0.19, respectively.**Table 2.** Summary of simulations used in this paper

Model	mesh <sup>a</sup> size	particles <sup>b</sup>	box size <sup>c</sup> ( $h^{-1} \text{ Mpc}$ )	resolution <sup>d</sup> ( $h^{-1} \text{ kpc}$ )	realizations <sup>e</sup>
SCDM	$768^3$	$384^3$	300	390	1
$\Lambda\text{CDM}_{0.3}$	$512^3$	$256^3$	200	390	3
$\Lambda\text{CDM}_{0.4}$	$512^3$	$256^3$	200	390	3
$\text{TACDM}_{0.4}$	$768^3$	$384^3$	300	390	1
$\text{TACDM}_{0.4}$	$512^3$	$256^3$	100	195	3
$\text{TACDM}_{0.4}$	$512^3$	$256^3$	50	98	3
$\Lambda\text{CDM}_{0.5}$	$768^3$	$384^3$	300	390	1
$\text{CHDM}_{0.7}$	$768^3$	$3 \times 256^3$	255	332	1
$\text{CHDM}_{0.8}$	$768^3$	$3 \times 384^3$	300	390	1

<sup>a</sup> Total number of PM divisions.<sup>b</sup> Number of particles in the box.<sup>c</sup> Total size of the box.<sup>d</sup> Box size divided by the number of PM divisions.<sup>e</sup> Number of simulations with different realizations that were averaged.

the region  $0.015 < k < 1 h \text{ Mpc}^{-1}$ . Power spectra from three catalogs of galaxies in redshift-space were used: the Stromlo/APM survey (Loveday et al. 1992); the CfA survey (Vogeley et al. 1992); and *IRAS* galaxies from the QDOT sample (Feldman et al. 1994). A straight mean of the two power spectra in the CfA paper was taken. Two catalogs of clusters of galaxies in redshift-space were used, the power spectrum of Abell clusters of richness class 1 or higher (Peacock & West 1992) and the power spectrum of radio galaxies from (Peacock & Nocholson 1991) The two cross-correlations are between *IRAS* galaxies and Abell clusters and between *IRAS* galaxies and radio galaxies (Mo et al. 1993).

Different biases should be assigned to the different data sets based on how they were selected. PD94 defined four adjustable bias parameters for the four categories in this sample:  $b_A$  for Abell clusters,  $b_R$  for radio galaxies,  $b_O$  for

optically-selected galaxies, and  $b_I$  for *IRAS* galaxies. Using a likelihood method, PD94 chose the ‘best’ ratio of these bias parameters to be

$$b_A : b_R : b_O : b_I = 4.5 : 1.9 : 1.3 : 1.0, \quad (6)$$

normalized to  $b_I = 1$ . In this paper we adopt the above ratio but use  $b_I$  as a reference level which can be adjusted. The necessity of this step will be discussed in §6.

This sample well represents the observable power spectrum in the quasi-nonlinear regime up to such small  $k$  that there should be no apparent nonlinear effects. The method that is described in the following section performs very well in this region of the power spectrum. Using this method we will attempt to remove all of the observational effects from these power spectra.

## 4 METHOD

The linearization method that we use is wholly based on that of PD94 and the later modification by PD96 which improved the handling of CDM-type power spectra. In order to recover a pure linear spectrum from real observations three effects must be corrected for: redshift distortions, bias and nonlinear growth. In practice, corrections for the redshift distortions and bias are inseparable and are applied together through a single equation (§4.1). The resulting nonlinear spectrum can be mapped to the linear spectrum on the linear scale.

The contribution to the fractional density variance per bin of  $\ln k$ , denoted  $\Delta^2(k)$  (Peebles 1980), is related to the power spectrum  $P(k) = \langle |\delta_{\mathbf{k}}|^2 \rangle$  as

$$\Delta^2(k) = \frac{k^3}{2\pi^2} P(k). \quad (7)$$

### 4.1 Correcting for redshift distortions and bias

Kaiser (1987) gave an analytical form for the enhancement of the power spectrum due to the collapse of waves in the linear regime. For a single wave, the relation between real space  $\Delta_r^2$  and redshift space  $\Delta_z^2$  is

$$\Delta_z^2(k) = \Delta_r^2(k) \left[ 1 + \mu^2 \frac{f}{b} \right]^2, \quad (8)$$

where  $f$  is the linear growth rate of velocity

$$f(\Omega, \Lambda) \equiv \frac{d \ln \delta}{d \ln a} \approx \Omega^{0.6}, \quad (9)$$

$\mu$  is the direction cosine between the wave vector and the line of sight, and a scale-independent bias  $b$  is included. Averaged uniformly over all  $\mu$ , this relation becomes

$$\Delta_z^2(k) = \Delta_r^2(k) \left[ 1 + \frac{2}{3} \frac{f}{b} + \frac{1}{5} \frac{f^2}{b^2} \right]. \quad (10)$$

This formula describes the modification of the power spectrum on linear scales. On nonlinear scales, large random peculiar velocities within collapsed objects cause an apparent elongation in a direction along the line of sight ('fingers-of-God'), which decreases power on cluster-sized scales and smaller. Assuming that the velocity distribution is Gaussian, this modifies the power spectrum as

$$\Delta_z^2(k) = \Delta_r^2(k) \exp \left[ -\frac{1}{2} \left( \frac{\mu k \sigma}{H_0} \right)^2 \right] \quad (11)$$

where  $\sigma$  is the 1D rms velocity dispersion (Peacock 1992). When averaged over all angles, this gives

$$\Delta_z^2(k) = \Delta_r^2(k) \left[ \frac{\sqrt{\pi}}{2} \frac{\text{erf}(k\sigma/H_0)}{k\sigma/H_0} \right]. \quad (12)$$

PD94 combined Eq. (10) and (12) along with the galaxy bias into a single formula that is applicable on all scales and also allows for cross-correlation between power spectra from two different catalogues. This formula is

$$\Delta_r^2(k) = \Delta_z^2(k) [b_1 b_2 G(y, \alpha_1, \alpha_2)]^{-1} \quad (13)$$

where

$$y \equiv \frac{k}{100} \sqrt{(\sigma_1^2 + \sigma_2^2)/2}, \quad (14)$$

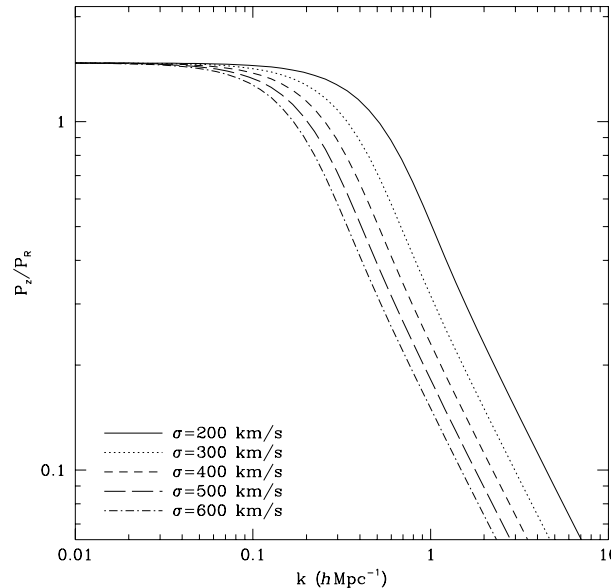


**Figure 1.** The redshift correction is plotted as a function of  $k$  and of the 1D velocity dispersion,  $\sigma$ , for the  $\Lambda\text{CDM}_{0.4}$  model with  $b = 1$ . On large scales the overall correction is that of Kaiser (1987) while on small scales corrections are due to the 'finger-of-God' effect, which is sensitive to  $\sigma$ . Notice that in the region  $k \gtrsim 0.1 h \text{ Mpc}^{-1}$ , a slightly higher or lower value could alter the correction noticeably.

$$\alpha \equiv f(\Omega)/b, \quad (15)$$

$$G(y, \alpha_1, \alpha_2) = \frac{\sqrt{\pi}}{8} \frac{\text{erf}(y)}{y^5} [3\alpha_1\alpha_2 + 2(\alpha_1 + \alpha_2)y^2 + 4y^4] - \frac{\exp(-y^2)}{4y^4} [\alpha_1\alpha_2(3 + 2y^2) + 2(\alpha_1 + \alpha_2)y^2], \quad (16)$$

and subscripts 1 and 2 refer to quantities for two different catalogues, in the case of a cross-correlation. Eq. (14) is for  $k$  in units of  $h \text{ Mpc}^{-1}$  and  $b$  is the bias. Eq. (13) is to be applied point by point to the raw observational power spectrum in redshift space. In the case of the APM spectrum,  $G$  must be taken as unity since there are no redshift-space distortions.

Because of Eq. (14) and (16), the redshift correction in Eq. (13) is sensitive to the velocity dispersion. PD94 make the approximation that  $\sigma = 300 \text{ km s}^{-1}$  for each of the catalogues in the data set. We note that a slightly different choice of  $\sigma$  could significantly affect the redshift correction at  $k \gtrsim 0.1 h \text{ Mpc}^{-1}$ . In Figure 1 we show how Eq. (13) appears when several different values of the velocity dispersion are chosen for the  $\Lambda\text{CDM}_{0.4}$  model. For example, the correction at  $k = 1 h \text{ Mpc}^{-1}$  is about 40 per cent greater for  $\sigma = 400 \text{ km s}^{-1}$  than for  $\sigma = 300 \text{ km s}^{-1}$ .

We are able to test the accuracy of the redshift corrections using our simulations. We placed dark matter particles from the  $\Lambda\text{CDM}_{0.4}$  model at the  $z = 0$  moment into redshift space according to Hubble's law and the peculiar motions of the particles. Then we calculated the power spectrum from two different vantage points within the box and averaged together all of these power spectra from each of the realizations of a particular box size. By taking the ratio of the redshift space power spectrum to the real space power spectrum, we produced a redshift correction for the model which can be directly compared with the prediction

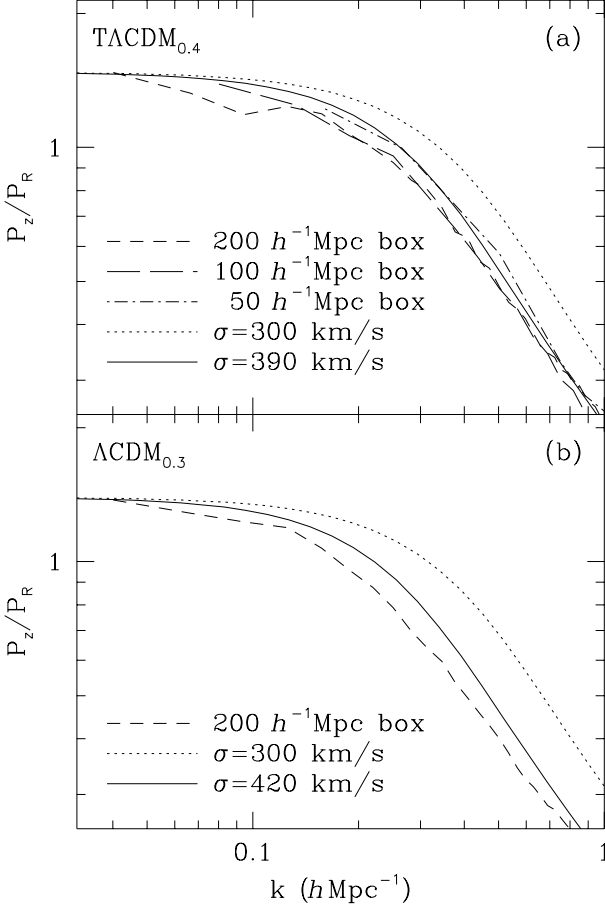


**Figure 2.** The redshift correction vs.  $k$  as verified with simulations. Two models were tested, (a)  $\text{TACDM}_{0.4}$  and (b)  $\Lambda\text{CDM}_{0.3}$ , both with  $b = 1$ . The results for different box sizes (broken lines) are plotted along with the analytical predictions of Eq. (13) (solid and dotted lines) for two different values of  $\sigma$ . It can plainly be seen that the corrections based on  $\sigma$  taken from the simulations give much better fits than the straight  $\sigma = 300 \text{ km s}^{-1}$  of PD94.

of Eq. (13), which is presented in Figure 2. Two different theoretical predictions are shown, the PD94 prediction with  $\sigma = 300 \text{ km s}^{-1}$  and a prediction curve using the average velocity dispersion from simulations of the largest boxes for each model. Clearly, the simulated corrections conform better to the prediction using the actual velocity dispersion than the PD94's assumed value of  $\sigma = 300 \text{ km s}^{-1}$ . We conclude that this is an important effect which *must* be included in this type of analysis, and we will therefore apply redshift corrections based on the 1D velocity dispersions from simulations throughout this paper.

In order to arrive at 1D velocity dispersions that are appropriate for the models that we test in this paper, we examined all models that have  $300 h^{-1} \text{ Mpc}$  boxes. We calculated the rms velocity dispersion of all particles in the boxes and computed the redshift correction to the power spectrum as described above. We found the following 1D velocities to be representative of the three families of models considered:  $610 \text{ km s}^{-1}$  for SCDM,  $430 \text{ km s}^{-1}$  for  $\Lambda\text{CDM}$ , and  $540 \text{ km s}^{-1}$  for CHDM. These numbers are used for  $\sigma$  throughout the rest of the paper.

#### 4.2 Correcting for nonlinear growth

By extending the method of HLKM from the correlation function to the power spectrum, PD94 arrived at a fitting formula that would relate the linear to the nonlinear spectrum. This procedure has two parts: adjusting the amplitude of the power spectrum, and transforming between the linear and nonlinear scales. Originally it was thought that the linear–nonlinear mapping would be nearly model-independent, with the density parameters being the only information about the model to enter into the equations (cf. PD94). However, later investigation by Jain, Mo, & White (1995) showed that there was a significant dependence on the slope of the linear power spectrum as well. We chose to adopt the new method of PD96 with small modifications for performing the linear–nonlinear mapping.

We assume that the linear  $\Delta_L^2(k)$  is related to the nonlinear  $\Delta_{\text{NL}}^2(k)$  through

$$\Delta_{\text{NL}}^2(k_{\text{NL}}) = f_{\text{NL}}(\Delta_L^2(k_{\text{L}})) \quad (17)$$

where  $f_{\text{NL}}$  is a fitting function of the form

$$f_{\text{NL}}(x) = x \left[ \frac{1 + B\beta x + [Ax]^{\alpha\beta}}{1 + ([Ax]^{\alpha} g^3(\Omega)/[Vx^{1/2}])^{\beta}} \right]^{\frac{1}{\beta}}. \quad (18)$$

This formula has an explicit dependence on  $\Omega$  through the growth suppression factor  $g(\Omega, \Lambda)$ , given in Eq. (2), and five free parameters. The best-fitting parameters were determined by PD96 to be

$$A = 0.482(1 + n/3)^{-0.947}, \quad (19)$$

$$B = 0.226(1 + n/3)^{-1.778}, \quad (20)$$

$$\alpha = 3.310(1 + n/3)^{-0.244}, \quad (21)$$

$$\beta = 0.862(1 + n/3)^{-0.287}, \quad (22)$$

$$V = 11.55(1 + n/3)^{-0.423}, \quad (23)$$

which are all dependent on the local slope of the linear power spectrum,

$$n \equiv \frac{d \ln P}{d \ln k}. \quad (24)$$

In addition to a change of amplitude there must also be a change of scale. As linear perturbations become nonlinear, objects with density contrast  $1 + \delta$  have collapsed radially by a factor of  $(1 + \delta)^{1/3}$ . This suggests that the scale  $k_{\text{NL}}$  is related to the scale  $k_{\text{L}}$  by the equation

$$k_{\text{NL}} = [1 + \Delta_{\text{NL}}^2(k_{\text{L}})]^{1/3} k_{\text{L}}. \quad (25)$$

Taken together, Eqns. (17) and (25) and their attending equations comprise the nonlinearization process, which predicts the observed nonlinear power spectrum in redshift space from a given linear spectrum in real space.

A more useful applications of these methods would be the inverse process – linearization. Eq. (13) can simply be solved for  $\Delta_{\text{r}}^2(k)$  and the fitting formula in Eq. (18) can be inverted numerically. The change of scale expressed in Eq. (25) can be stated equivalently as

$$k_{\text{L}} = [1 + \Delta_{\text{NL}}^2(k_{\text{NL}})]^{-1/3} k_{\text{NL}}, \quad (26)$$

completing the tool set for use in manipulating the power spectrum.

This method works well for scale-free power law spectra with a constant slope  $n$  of the linear  $P(k)$ , but not for scale-dependent power spectra. The curving shape of CDM-type power spectra could not be reconstructed with much success. Jain et al. (1995) suggested that CDM-type spectra could be treated by choosing a constant ‘effective’ slope,  $n_{\text{eff}}$ , to take the place of  $n$  in Eqns. (19–23). The effective slope is defined as the tangent slope of the linear  $P(k)$  at the nonlinear scale (where the mass fluctuation is unity). A linearization using  $n_{\text{eff}}$  can only approximate the true shape of the linear spectrum since the method is based on deriving the linear power from the nonlinear power on a smaller scale. Because the slope of the CDM-type spectrum is always changing, the effective index should continually change with scale, as was recognized by PD96. We choose  $n$  from the linear power spectrum on the appropriate linear scale  $k_L$  by numerically differentiating  $P(k_L)$ , which works reasonably well.

## 5 APPLICATION OF THE METHOD TO SIMULATIONS

In order to thoroughly test this method, we applied it to our database of simulations or ran new simulations suitable for this purpose. For each realization listed in Table 2, we calculated the nonlinear power spectrum at the moment  $z = 0$  and then averaged them together for each box size. For the  $\text{TACDM}_{0.4}$  model, which has multiple box sizes, we constructed a complete nonlinear power spectrum by combining the spectra starting with the power from the largest box size and adding power from successively smaller boxes multiplied by a small factor if needed (to account for power from missing long waves).

With this information we could test the procedure in either of two ways: linearizing the nonlinear power spectrum and then comparing it to the linear power spectrum of the model, or nonlinearizing the generated linear power spectrum and then comparing it to the actual nonlinear spectrum from simulations. In fact, we did both so that we could demonstrate the consistency of both approaches. We tested the linear–nonlinear corrections of §4.2 on the final nonlinear and linear power spectra of the models. The results are presented in Figure 3 for all of the models that we used with the exception of  $\Lambda\text{CDM}_{0.4}$  (since it is very similar to  $\text{TACDM}_{0.4}$ ). These plots incorporate the shifted mapping  $n_L(k_L) \rightarrow n_L(k_L/2)$  from PD96. All models appear to fit quite well over the entire range in scales that we have been able to faithfully simulate.

Figure 4 presents the relation between  $\Delta_{\text{NL}}^2$  and  $\Delta_L^2$ . This format removes  $k$  dependence by plotting the linear–nonlinear mapping only. This allows a more careful examination of the goodness of fit than the previous Figure. In addition to plotting the shifted linear–nonlinear mapping of PD96, the mapping with no shift in  $n_L(k_L)$  is plotted for comparison. We find that most models favor the shifted mapping except for  $\Lambda\text{CDM}_{0.4}$  model which clearly favored no shift, for which we have no explanation.

## 6 APPLICATION OF THE METHOD TO OBSERVATIONS

Now that a reliable linearization method has been designed and tested, it can be applied to real data in an attempt to constrain the models that best represent the Universe. As opposed to linearizing the observational data based on an arbitrary model and then comparing the linear power of a model in question with the linearized spectrum (PD94, Ma 1996), a particular model was applied to the observational data and the linearization was performed according to the specific theoretical predictions of that model. The most correct model should be identifiable by self-consistency: an exceptionally good fit of the linearized observations to the theoretical linear spectrum.

We adopted the same compilation of observational power spectra and error estimates as in PD94. For each data set we applied the linearization procedure for each cosmological model to correct for redshift distortions (except in the case of APM data), bias, and nonlinear effects. Once all data sets were linearized, the collective sample of power spectrum data points were averaged in bins  $0.1 \log_{10} k$  wide. The bin widths and centers were chosen to be nearly identical to those of PD94 in their Table 1. The resulting plots appear in Figure 5 and are discussed below.

Our approach in treating errors is different from PD94. They simply accepted errors based on counting statistics in bins, thus neglecting internal errors of the data sets. We attempted to keep track of individual error bars throughout the linearization process, assuming that errors of points in each data set are independent. This is not actually true, but it is difficult to estimate how the data points correlate. The error estimates were made in the following way. When performing redshift and bias corrections, the data points were simply scaled up or down by a factor (Eq. (13)), so the error estimates were simply scaled by the same factor. For the case of nonlinear corrections, we performed the correction on both  $\Delta^2$  and the upper limit  $\Delta^2 + \delta$  and used the difference between these two corrected points as the error estimate. Technically, this gives an error at a different  $k$  than the data point in question, which has the effect of reducing the size of the error. However, since the original errors are uncertain to begin with, we expect that our final estimates are at least a fair representation of the errors. Correlations in the observational data points will lead to the plotted errors being an underestimate of the true errors.

While we assumed the same relative biases as PD94 (Eq. (6)), the biases were all scaled by the same constant so that the linearized spectrum obtained from observational data could be best fit to the linear dark matter spectrum according to a  $\chi^2$  test. Each bias in Eq. (6) was multiplied by this factor, reflected in the value of  $b_I$ , before being applied to the observational data through Eq. (13). Table 3 gives the best  $b_I$  for each model as well as an indicator meant to quantify the goodness of fit of the linearizations. The indicator (called the ‘ $P$  ratio’) is the average of the ratio of linear power to linearized power at three points near the middle of the sample,  $k = 0.071, 0.090$ , and  $0.113 h \text{ Mpc}^{-1}$ , chosen to be near the maximum curvature of the power spectra and have relatively small error bars. Since decreasing  $b_I$  moves the spectrum up and increases its curvature, this indicator should be a reliable estimate of how close the curvature of

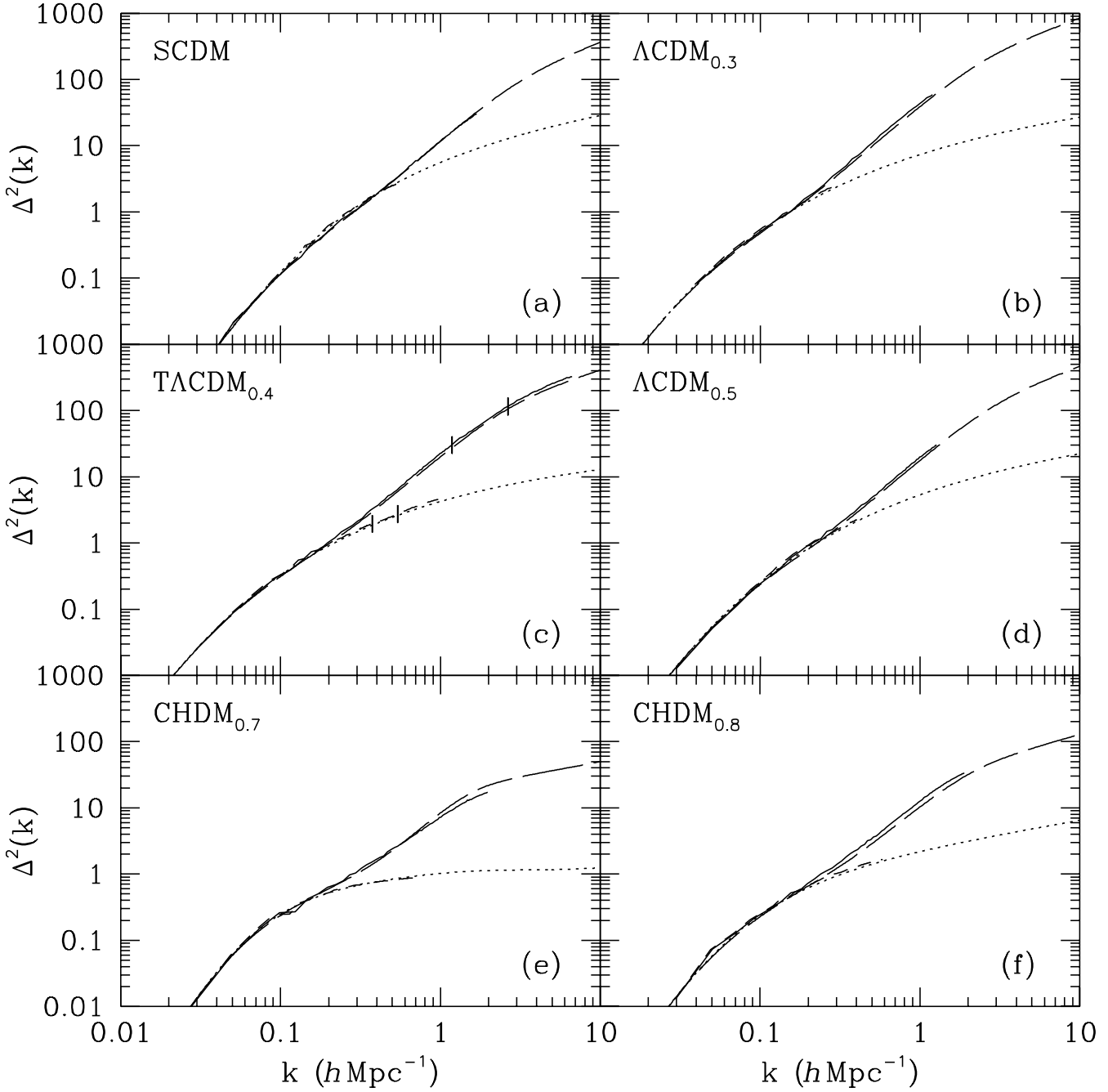


**Figure 3.** This figure plots the linear power spectrum for each model (dotted line) and the nonlinear power spectrum from simulations (solid line) against the linearized power spectrum (short dashed line) and the nonlinearized power spectrum (long dashed line). The linearized and nonlinearized lines are from the application of the method described in §4, with a modification of the local slope of the linear power spectrum  $n_L(k_L) \rightarrow n_L(k_L/2)$  as used in PD96. Because the TACDM<sub>0.4</sub> model has simulations with high resolution that sample smaller waves, it is plotted to higher values of  $k$ . The short horizontal lines denote boundaries between the 300, 100, and 50  $h^{-1}$  Mpc samples. At high values of  $k$  resolution effects in the simulations bring the power spectrum lower than what it should be. We chose to stop plotting curves once  $\Delta^2(k)$  turned over.

the linearized spectrum is to matching that of the linear power spectrum for the model. In the case where the curvature is very different, however, the  $P$  ratio tends to be low (since the two best-fitting curves intersect at the mid-point) giving a false indication of a good fit. In our sample of models, the  $P$  ratio for the SCDM model is the only one to

suffer from this problem because the SCDM power spectrum simply has the wrong shape.

Note that the last few (i.e., highest  $k$ ) binned points are always less reliable than the error bars indicate. They are either averages of only the APM and CfA results or of APM alone and have few points per bin. Quite often (e.g., Liddle et al. 1996a) the highest- $k$  points are ignored because the

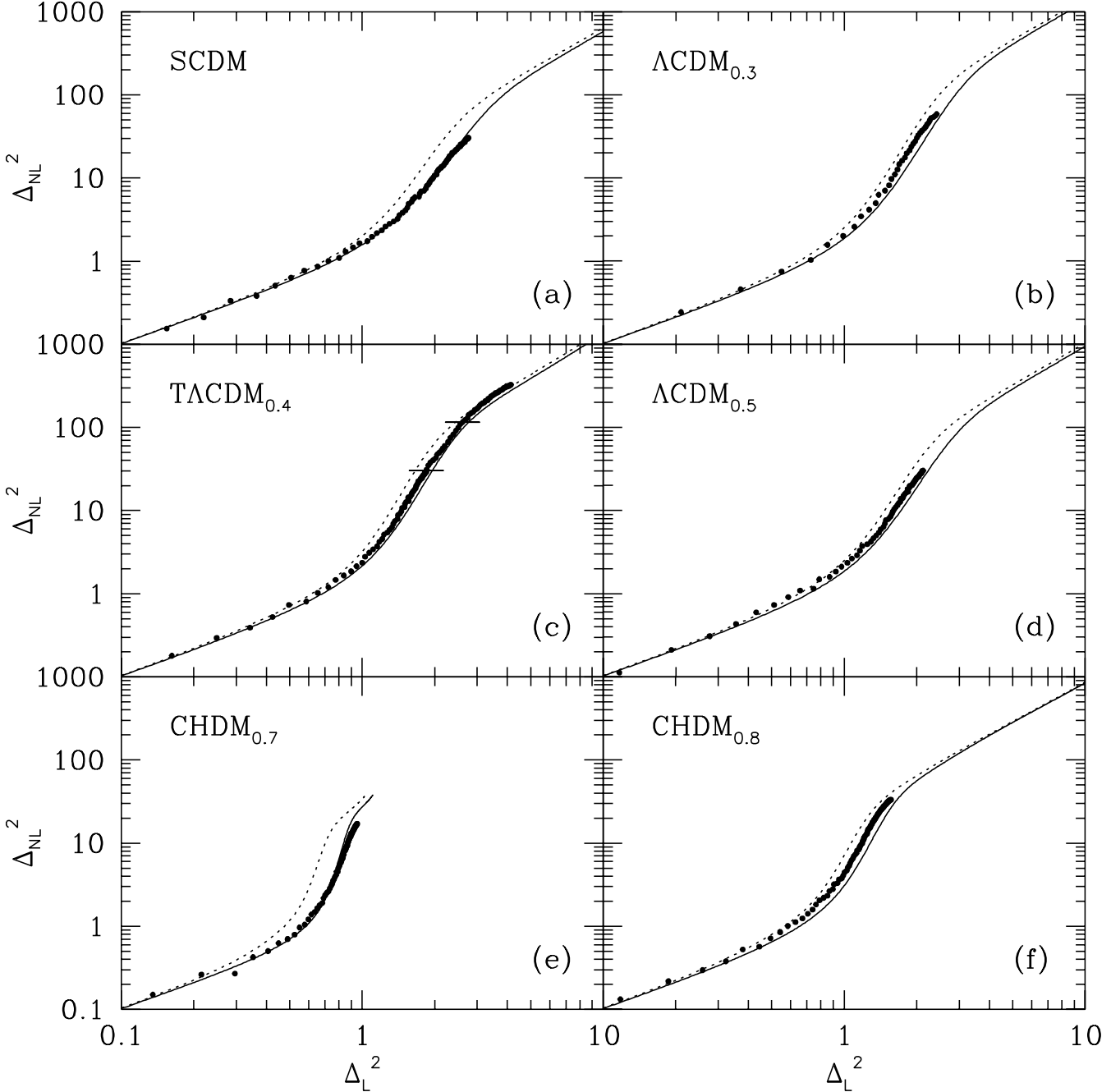


**Figure 4.** The effects of using shifted or unshifted  $n$  on the linear–nonlinear mapping. The solid line represents the mapping in Eq. (18) performed without a shift while the dotted line represents the mapping with a shift of a factor of 2, as in PD96. The filled circles show the linear–nonlinear relation of the real-space power spectrum from simulations of the models.

earlier linearization algorithms were not accurate for these points. However, we think that these points should be included in the analysis as long as there are enough data points in the bins. They have the smallest statistical error bars and now cannot be excluded solely on the basis of failure of the linearization procedure, since our method demonstrably works up to this range in  $k$ .

We find that the  $\Lambda$ CDM family of models have the wrong shape when the best fitting bias  $b_1$  is determined. All of these models have too much curvature and fit poorly at the high- $k$  tail of points, even though most of the points

are within the nominal error bars. As  $b_1$  is lowered below unity, the curves of the reconstructed linear power spectra rise in amplitude and increase in curvature, which is what is responsible for the relatively poor fits. The reconstructed CHDM models both seem to do an exceptionally good job of fitting their respective power spectra. The excellent match of the curvature and the small adjustment to the bias make CHDM the most successful class of candidate models in our sample.

Because the  $\Lambda$ CDM power spectra did not fit well, we tried examining the effects of another possible modification

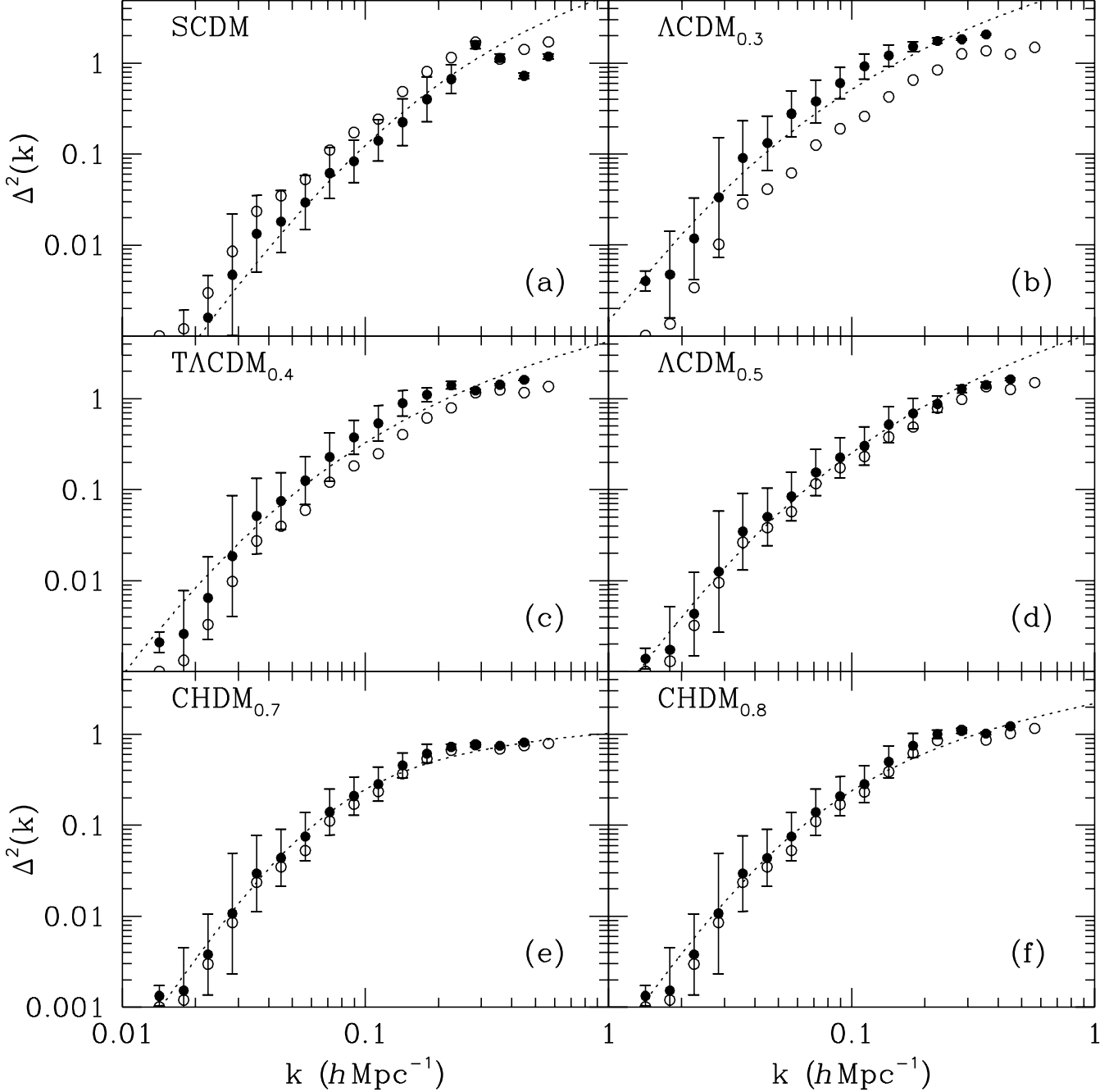


**Figure 5.** The application of the linearization technique to the observational data set. The linear power spectrum of the imposed model (dotted line) and two different cases of bias parameters are plotted (dots with error bars). The open dots correspond to the bias level of PD94 (Eq. (6) in this paper) and the filled dots are for the bias level adjusted by the factor given in Table 3, as determined by minimizing  $\chi^2$ . Error bars represent internal errors of each point in the bin added in quadrature. See the text for a more detailed explanation.

process. The formalism of §4.1 assumes that the bias does not change with scale. This is a useful first approximation, but may prove to be an oversimplification. It is quite possible that the bias depends on scale. Preliminary results from sophisticated  $N$ -body plus hydro simulations of galaxy formation done by Yepes et al. (1996) (which include multi-phase treatment of gas and supernovae feedback) indicate that bias is slightly rising with  $k$  for both CDM and  $\Lambda$ CDM models. The semi-analytic merging hierarchy inclusion of hydrodynamic effect in simulations by Kauffmann, Nusser,

& Steinmetz (1995) gave similar results regarding scale dependence of bias. In order to obtain a rough estimate of the possible effect we introduce a very simple model for bias which modifies the redshift-space correction of Eq. (13). Figure 6 shows the form of a bias which increases with scale in (a) and which decreases with scale in (b). It is a linear function of  $k$ :  $b_I = 1 + k_{NL}/(1 \text{ } h \text{ Mpc}^{-1})$  which is a factor of two at  $k_{NL} = 1 \text{ } h \text{ Mpc}^{-1}$ . Panel (c) shows that an extra positive bias makes the best fit even worse while (d) shows that anti-bias improves the best fit by raising the high- $k$  tail. Because

**Table 3.** Summary of best-fit biases

Model	$b_I^a$	$1.3b_I^b$	$b_O^c$	$P$ ratio <sup>d</sup>
SCDM	1.42	1.85	$1.35 \pm 0.24$	0.98
$\Lambda\text{CDM}_{0.3}$	0.50	0.64	$0.69 \pm 0.12$	1.41
$\Lambda\text{CDM}_{0.4}$	0.58	0.75	$0.81 \pm 0.14$	1.34
$\Lambda\text{ACDM}_{0.4}$	0.69	0.90	$0.81 \pm 0.14$	1.33
$\Lambda\text{CDM}_{0.5}$	0.85	1.11	$0.92 \pm 0.16$	1.09
$\text{CHDM}_{0.7}$	0.87	1.13	—	0.99
$\text{CHDM}_{0.8}$	0.87	1.13	—	1.04

<sup>a</sup> Factor by which the PD94 bias must be multiplied to achieve best fit.

<sup>b</sup> Bias of blue galaxies as indicated by the best fit  $b_I$ .

<sup>c</sup> Bias of blue galaxies from POTENT analysis Hudson et al. (1995).

<sup>d</sup> Average of  $P_{\text{linear}}/P_{\text{linearized}}$  at  $k = 0.071, 0.090$ , and  $0.113 h \text{ Mpc}^{-1}$ .

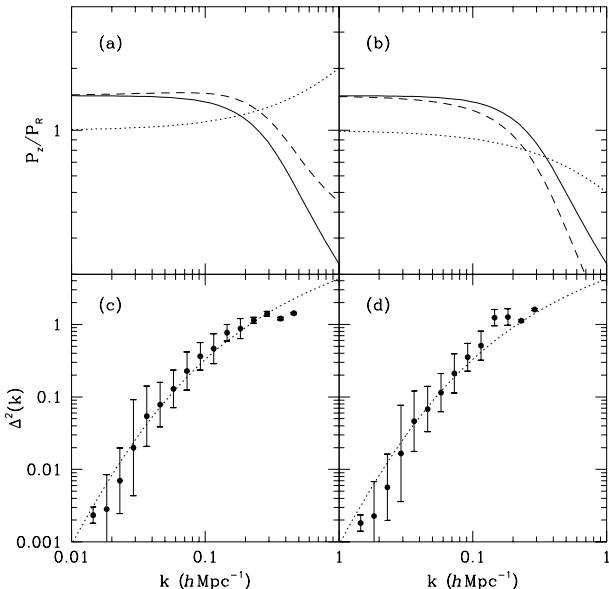


**Figure 6.** Test forms of scale-dependent bias and their effects on the recovered linear power spectrum for TACDM<sub>0.4</sub>. The solid line is the redshift correction of Eq. (13), the dotted line is the scale-dependent bias function and the dashed line is the application of the function to the redshift correction. (a) Bias increasing linearly with scale to a factor of 2 at  $k = 1$ . (b) Bias decreasing linearly with scale to a factor of 2 at  $k = 1$ . (c) The positive bias increases the curvature requiring more antibias. (d) The antibias decreases the curvature requiring less antibias.

such a large anti-bias is difficult to motivate physically, we do not regard it as an acceptable solution to this problem (cf. KPH96).

At this point we can demonstrate that the choice of 1D velocity dispersion has an impact on the form of a reconstructed linear power spectrum, as was argued in §4.1. Figure 7 shows that the velocity dispersion separates the different cases at the high- $k$  tail for the unbiased TACDM<sub>0.4</sub> model. Three realistic values of  $\sigma$  were chosen, 300 km s<sup>-1</sup> as in PD94, 430 km s<sup>-1</sup> as was used for all  $\Lambda\text{CDM}$  models, and 560 km s<sup>-1</sup> which is representative of CHDM models. Since for  $k > 0.2 h \text{ Mpc}^{-1}$  the curves are separated by an

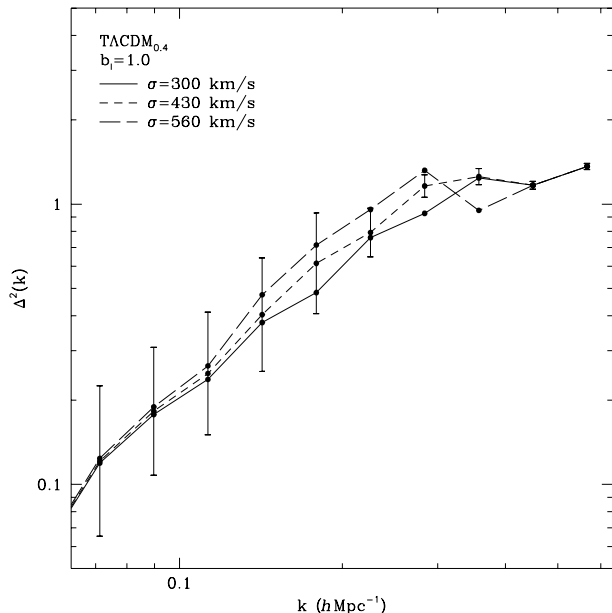


**Figure 7.** The effect of different choices of 1D velocity dispersion on the reconstructed observational TACDM<sub>0.4</sub> power spectrum. Error bars have been included for the  $\sigma = 430 \text{ km s}^{-1}$  case only, but are representative of the other cases. Only the high- $k$  points are shown since the differences are minimal at low  $k$  (see Figure 1). The last two points are degenerate for all values of  $\sigma$  since they are constructed from APM data only, which are not affected by the redshift correction.

amount greater than the error bars, the redshift correction can have a noticeable effect on the amplitude of the reconstructed power spectrum.

An interesting thing that we noticed was that the reconstructed observational power spectra of our  $\Lambda\text{CDM}$  models were virtually identical. The TACDM<sub>0.4</sub> model was the only exception (because of the tilt), but the difference is small. Figure 8, shows the average of the  $\Lambda\text{CDM}_{0.3}$ ,  $\Lambda\text{CDM}_{0.4}$  and  $\Lambda\text{CDM}_{0.5}$  models along with the TACDM<sub>0.4</sub> model for  $b_I$  values 1.0, 0.8 and 0.6. Using this to analyze the fit of the general  $\Lambda\text{CDM}$  spectrum, the averaged reconstructed  $\Lambda\text{CDM}$  spectrum for the same three  $b_I$  values overlaid by the linear power spectra of all of the  $\Lambda\text{CDM}$  models are shown in Figure 9. Again, this figure demonstrates that no level of constant  $b_I$  can provide an adequate reconstruction of the linear power spectrum for the  $\Lambda\text{CDM}$  models: the shape of the spectrum is not optimal.

A similar finding is that there is a universal linear power spectrum reconstructed from the observational data. Reconstruction for all models that we examined resulted in practically the same spectrum in the range  $0.01 \lesssim k \lesssim 0.1 h \text{ Mpc}^{-1}$ . Figure 10 shows that all models share an almost identical shape and amplitude in this region. This means that any future progress in distinguishing between these models will need to be emphasize nonlinear scales  $k \gtrsim 0.2 h \text{ Mpc}^{-1}$ . The data shown in Figure 10 have been tabulated in Tables 4–6.

They contain the linearized observational power spectra for the  $\Lambda\text{CDM}$ , CHDM, and SCDM models, respectively.

**Table 4.**  $\Lambda$ CDM family of recovered linear power spectra  $\Delta^2(k) = \frac{k^3}{2\pi^2} P(k)$ 

$k, (h \text{ Mpc}^{-1})$	$b_I = 0.6$		$b_I = 0.8$		$b_I = 1.0$	
	$\Lambda$ CDM	TACDM	$\Lambda$ CDM	TACDM	$\Lambda$ CDM	TACDM
0.0142	0.0028	0.0028	0.0016	0.0016	0.0010	0.0010
0.0179	0.0033	0.0033	0.0020	0.0020	0.0013	0.0013
0.0225	0.0082	0.0082	0.0050	0.0049	0.0033	0.0033
0.0284	0.0234	0.0234	0.0145	0.0145	0.0098	0.0098
0.0357	0.0641	0.0638	0.0400	0.0400	0.0274	0.0273
0.0450	0.0935	0.0932	0.0583	0.0582	0.0397	0.0397
0.0566	0.156	0.155	0.0970	0.0969	0.0597	0.0597
0.0713	0.275	0.269	0.179	0.178	0.121	0.121
0.0897	0.461	0.456	0.270	0.273	0.182	0.182
0.113	0.639	0.624	0.387	0.387	0.248	0.249
0.142	0.942	0.921	0.621	0.611	0.406	0.403
0.179	1.17	1.14	0.857	0.845	0.593	0.615
0.225	1.72	1.63	1.15	1.16	0.821	0.792
0.284	1.53	1.33	1.39	1.30	1.17	1.16
0.357	1.80	1.62	1.37	1.22	1.36	1.25
0.450			1.67	1.52	1.26	1.17
0.566					1.49	1.36

**Table 5.** CHDM recovered linear power spectra  $\Delta^2(k) = \frac{k^3}{2\pi^2} P(k)$ 

$k (h \text{ Mpc}^{-1})$	$b_I = 0.8$		$b_I = 1.0$	
	CHDM <sub>0.7</sub>	CHDM <sub>0.8</sub>	CHDM <sub>0.7</sub>	CHDM <sub>0.8</sub>
0.0142	0.0016	0.0016	0.0010	0.0010
0.0179	0.0018	0.0018	0.0012	0.0012
0.0225	0.0044	0.0044	0.0030	0.0030
0.0284	0.0122	0.0122	0.0085	0.0085
0.0357	0.0336	0.0336	0.0237	0.0237
0.0450	0.0500	0.0499	0.0350	0.0350
0.0566	0.0863	0.0861	0.0530	0.0529
0.0713	0.159	0.158	0.111	0.111
0.0897	0.236	0.236	0.170	0.169
0.113	0.341	0.350	0.235	0.233
0.142	0.537	0.615	0.368	0.388
0.179	0.647	0.813	0.540	0.619
0.225	0.768	1.11	0.666	0.854
0.284	0.797	1.15	0.768	1.11
0.357	0.762	1.06	0.690	0.868
0.450	0.830	1.26	0.750	1.03
0.566			0.795	1.16

## 7 CONCLUSIONS

We have reconstructed the linear power spectra from observations for several current cosmological models based on rigorously tested linearization methods. We have found that:

(i) The linearized power spectra of all  $\Lambda$ CDM and CHDM models are systematically below their respective linear power spectra using the bias ratio in Eq. (6) normalized so that the bias of *IRAS* galaxies  $b_I = 1.0$ . It was necessary to adjust the normalization of the bias ratio so that  $b_I < 1.0$  to obtain the best fit. While this implies that optically selected galaxies must be antibiased ( $b_O < 1$ ) to be consistent with models, this may be acceptable since a recent POTENT analysis (Hudson et al. 1995) allows a slight antibias for some  $\Lambda$ CDM models.

(ii) The linearization of the SCDM model cannot be made to fit its linear power spectrum under any circumstances and fits very poorly at best. This simply reconfirms the incompatibility of SCDM with observations, as has long been recognized.

(iii) The  $\Lambda$ CDM models all appear moderately successful, as indicated by our ‘ $P$  ratio’ indicator in Table 3, but share difficulties in matching the shape of their linear spectra. This is a consequence of our finding that the linearized spectra of all  $\Lambda$ CDM models share a common shape for a given bias. The only exception is the TACDM<sub>0.4</sub> model, though it deviates from the others by at most 10 per cent at  $k \sim 0.5 h \text{ Mpc}^{-1}$ . This is to be expected since TACDM<sub>0.4</sub> has more curvature by design. The best fitting  $\Lambda$ CDM model is  $\Lambda$ CDM<sub>0.5</sub> as determined from Table 3.

(iv) The CHDM models seem to do an excellent job of recovering their linear power spectra from observations. They require relatively small  $b_I$  to fit well and have the lowest  $P$  ratios. Ma (1996) found that a slight tilt of  $n = 0.9$ –0.95 is needed to bring  $h = 0.5$  CHDM models into agreement with the PD94 reconstructed spectrum. However, if one reconstructs the linear spectrum self-consistently, using the nonlinear spectrum for the CHDM models considered here, there is good agreement without any tilt.

(v) There are physical motivations to include a scale-

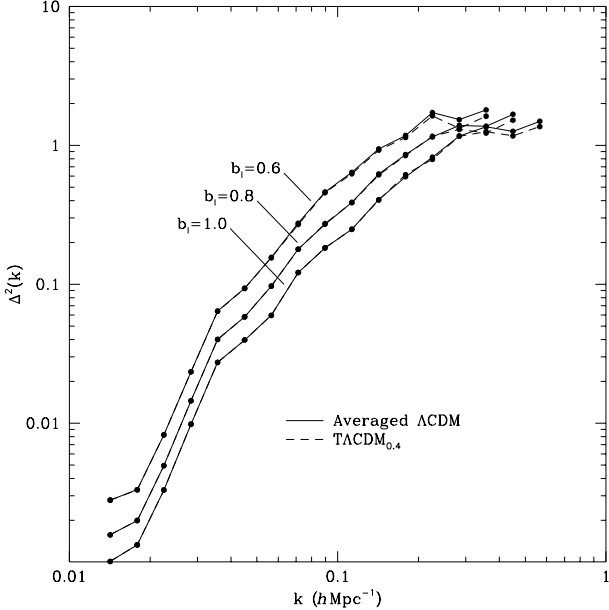


**Figure 8.** Observational linear power spectrum reconstructed under an assumption that the Universe is of a  $\Lambda$ CDM type. Because the reconstructed spectra were very similar for  $\Lambda$ CDM<sub>0.3</sub>,  $\Lambda$ CDM<sub>0.4</sub>, and  $\Lambda$ CDM<sub>0.5</sub> models, we present averaged spectra for assumed level of bias. The spectrum reconstructed assuming the TACDM<sub>0.4</sub> models differ slightly from the rest and are drawn as dashed lines. These data points are given in Table 4.

**Table 6.** SCDM recovered linear power spectra  $\Delta^2(k) = \frac{k^3}{2\pi^2} P(k)$

$k$ ( $h$ Mpc $^{-1}$ )	$b_I = 0.6$	$b_I = 0.8$	$b_I = 1.0$
0.0142	0.0028	0.0016	0.0010
0.0179	0.0028	0.0018	0.0012
0.0225	0.0071	0.0044	0.0030
0.0284	0.0189	0.0122	0.0085
0.0357	0.0513	0.0335	0.0236
0.0450	0.0765	0.0498	0.0349
0.0566	0.135	0.0861	0.0527
0.0713	0.237	0.159	0.111
0.0897	0.412	0.243	0.173
0.113	0.664	0.379	0.242
0.142	1.25	0.756	0.488
0.179	1.69	1.10	0.807
0.225	2.10	1.70	1.15
0.284	1.65	1.75	1.70
0.357	2.10	1.50	1.11
0.450		1.94	1.42
0.566			1.71

dependent bias in the treatment of observational power spectra. Such a bias would increase with higher  $k$  and would make the reconstructions at  $k \gtrsim 0.2 h$  Mpc $^{-1}$  worse than they already are. A bias that decreased with scale could significantly improve the agreement between the assumed and reconstructed power spectrum for each model, especially the  $\Lambda$ CDM models, but this appears to be an entirely ad hoc assumption.

(vi) There is a unique model-independent linear power spectrum that can be recovered from observations in the

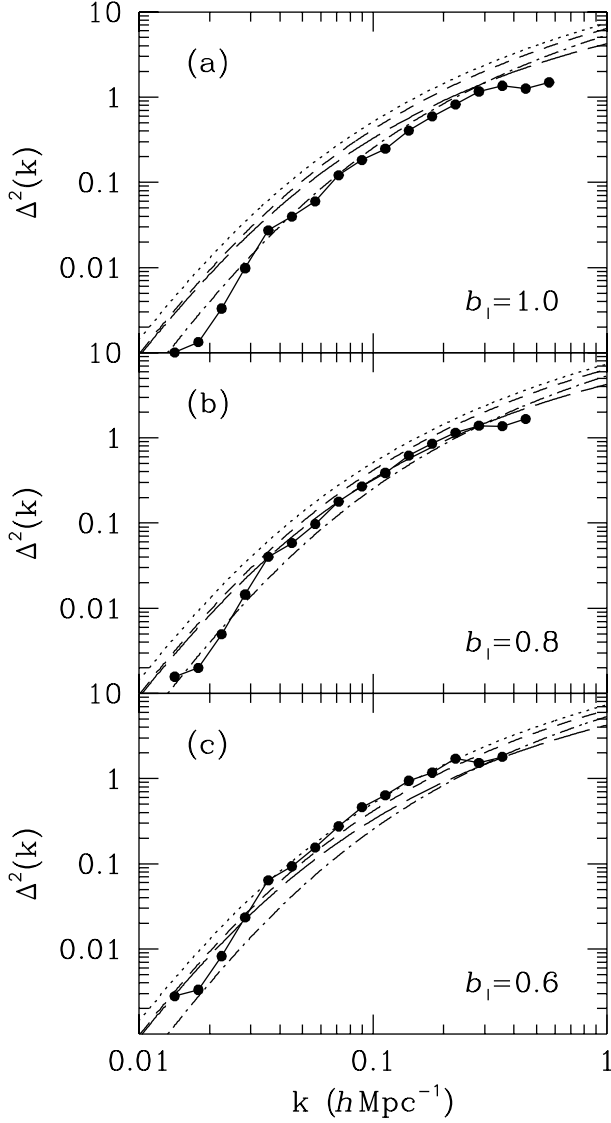


**Figure 9.** Comparison of averaged  $\Lambda$ CDM<sub>0.3</sub>,  $\Lambda$ CDM<sub>0.4</sub> and  $\Lambda$ CDM<sub>0.5</sub> simulations with linearized observational power spectra appropriate to  $\Lambda$ CDM cosmology for different biases. Dotted lines depict the linear power spectrum of  $\Lambda$ CDM<sub>0.3</sub>, short dashed lines depict  $\Lambda$ CDM<sub>0.4</sub>, long dashed lines depict TACDM<sub>0.4</sub>, and dot-dashed lines depict  $\Lambda$ CDM<sub>0.5</sub>. The biases in the panels are (a)  $b_I = 1.0$ , (b)  $b_I = 0.8$ , and (c)  $b_I = 0.6$ .

region  $0.01 \lesssim k \lesssim 0.1 h$  Mpc $^{-1}$ , at least for the models considered here.

We have demonstrated that the linearization method is accurate to within 20 per cent up to linear scales of at least  $k = 1 h$  Mpc $^{-1}$  and possibly higher. Because the most favorable models are nearly identical up to the highest reliable bin, a power spectrum with small errors that extends from large nonlinear scales to  $k \sim 10 h$  Mpc $^{-1}$  or more would be very helpful in constraining the shape of theoretical linear power spectra.

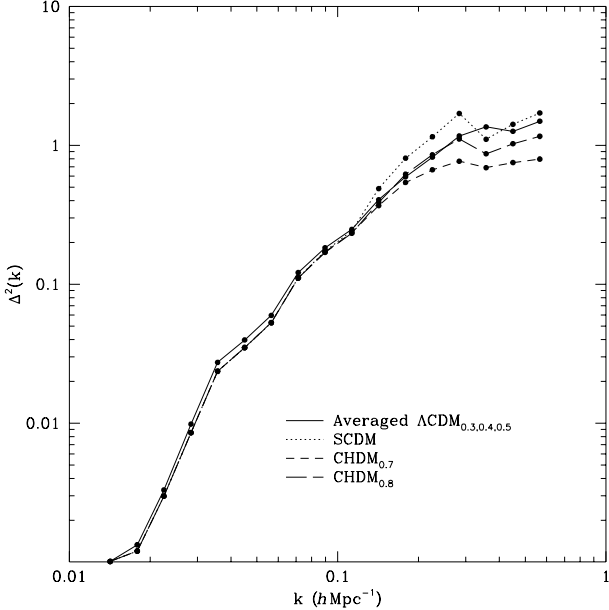


**Figure 10.** Comparison of different linearized observational power spectra with  $b_1 = 1.0$  in each case.

## ACKNOWLEDGEMENTS

Simulations were performed on the CM-5 and Convex 3880 at the National Center for Supercomputing Applications, University of Illinois, Champaign-Urbana, IL, and the SP2 at the Theory Center, Cornell University, Ithaca, NY. We acknowledge support from NSF and NASA grants at NMSU and UCSC.

## APPENDIX A: FITTING FUNCTIONS FOR LINEAR POWER SPECTRA

### A1 Calculations

The linear calculations were done using the techniques of Holtzman (1989). Perturbations in radiation, baryons, cold dark matter, and massive and massless neutrinos were calculated from a scale factor of  $1 \times 10^{-10}$  to the present (where the scale factor is  $a \equiv 1/(1+z)$ ). For models without massive neutrinos, three massless neutrino species were used; for models with massive neutrinos, the mass was either placed in a single neutrino species or two equal-mass species, with the other species remaining massless.

For the radiation, the angular dependence of the perturbations was handled by expanding the perturbation in Legendre polynomials,  $\delta_r = \sum \Delta_l(k, a) P_l(\cos\theta)$ . The calculation started with a small number of orders, but additional orders were added as they became needed to keep the final  $P(k)$  results accurate to 1 per cent. For large scales ( $k < 0.7 \text{ h Mpc}^{-1}$ ), the radiation perturbations were integrated all the way to the present. For smaller scales, they were integrated through recombination, and then the analytic solution presented by Bond and Efstathiou (1987) was used to calculate the perturbations at the present time; no approximations were made for any scale for the radiation perturbations. The recombination history of Peebles (1967)

was used for hydrogen, but a helium mass fraction of 0.25 was included.

For the massive neutrinos, the perturbations are a function of both angle and neutrino momentum. We calculated the evolution for 15 separate momenta up to the time when the neutrinos became nonrelativistic; this was done using the integro-differential equations presented by Bond and Szalay (1983). This technique allows only the 0th and 1st orders of the neutrino angular distribution to be computed without following higher orders; these are the only orders than enter as the gravitational source terms. For small scales, even this computation can get very expensive, so the massive neutrino perturbations were manually damped when they became gravitationally negligible (which occurs because the perturbations are destroyed by free-streaming). When the neutrinos became nonrelativistic, the full angular distribution for each momenta was calculated, and the subsequent evolution was computed using the full set of coupled differential equations exactly analogous to those used for the radiation perturbation.

### A2 Fitting functions

For convenience, we provide fits for the power spectrum of the hot and cold components as a function of wavenumber,  $k$ . For all of the calculations presented in this paper, we used the computed spectra directly, rather than the fits, to obtain results. The fits are good to better than 5 per cent in total power, in the worst case. Errors of 1–2 per cent are more typical for  $k = 0.1\text{--}30 \text{ h Mpc}^{-1}$ . For fitting functions, we used

$$P_{c+b}(k) = \frac{Ak^n}{(1 + a_1 k^{1/2} + a_2 k + a_3 k^{3/2} + a_4 k^2)^b} \quad (\text{A1})$$

for the cold and baryonic matter, and

$$P_\nu(k) = \frac{P_{c+b}(k) \exp(-ck^{1/2})}{(1 + d_1 k^{1/2} + d_2 k + d_3 k^{3/2} + d_4 k^2)^2} \quad (\text{A2})$$

for the massive neutrinos. The total power is given by

$$P(k) = \left[ \frac{\Omega_b + \Omega_c}{\Omega_0} \sqrt{P_{c+b}(k)} + \frac{\Omega_\nu}{\Omega_0} \sqrt{P_\nu(k)} \right]^2. \quad (\text{A3})$$

The parameters for all the models considered in this paper are presented in Table 7 for the cold component and in Table 8 for the hot component; the coefficients assume the use of units of  $\text{h Mpc}^{-1}$  for  $k$  in equations A1 and A2. The normalization  $A$  is set to reproduce the  $\sigma_8$  used in this paper.

## REFERENCES

Bardeen, J., Bond, J. R., Kaiser, N., & Szalay, A. S., 1986, *ApJ*, 304, 15 (BBKS)  
 Baugh, C. M., & Efstathiou, G., 1993, *MNRAS*, 265, 145  
 Borgani, S., Moscardini, L., Plionis, M., Gorski, K., Holtzman, J., Klypin, A., Primack, J.R., Smith, C.L. & Stompor, R. 1997, *New Astronomy*, in press; preprint astro-ph/9611100  
 Carroll, S. M., Press, W. H., & Turner, E. L., 1992, *ARA&A*, 30, 499

**Table 7.** Linear Power Spectra for Cold Matter at  $z = 0$ 

Model	$A (h^{-3-n} \text{ Mpc}^{3+n})$	$n$	$a_1$	$a_2$	$a_3$	$a_4$	$b$
$\Lambda\text{CDM}_{0.3}$	$4.507 \times 10^6$	1	-1.3050	33.590	68.973	157.74	1.8606
$\Lambda\text{CDM}_{0.4}$	$2.663 \times 10^6$	1	-1.2120	29.224	57.044	119.53	1.8623
$\text{TACDM}_{0.4}$	$1.697 \times 10^6$	0.9	-1.2120	29.224	57.044	119.53	1.8623
$\Lambda\text{CDM}_{0.5}$	$9.880 \times 10^5$	1	-1.0752	24.087	36.390	78.732	1.8533
$\text{CHDM}_{0.7}$	$5.960 \times 10^5$	1	-1.0421	19.270	-56.526	310.68	1.8270
$\text{CHDM}_{0.8}$	$7.827 \times 10^5$	1	-0.1828	0.4526	73.673	104.66	1.8571

**Table 8.** Linear Power Spectra for Hot Matter at  $z = 0$ 

Model	$c$	$d_1$	$d_2$	$d_3$	$d_4$
$\text{CHDM}_{0.7}$	0.65837	-0.51390	0.34412	0.032050	0.023225
$\text{CHDM}_{0.8}$	0.76462	-0.71510	1.6616	-1.0933	0.8900

Coble, K., Dodelson, S., & Frieman, J., 1996, preprint astro-ph/9608122

Feldman, H. A., Kaiser, N., & Peacock, J. A., 1994, ApJ, 426, 23

Hamilton, A. J. S., Kumar, P., Lu, E., & Matthews, A., 1991, ApJ, 374, L1 (HKLM)

Hockney, R. W., & Eastwood, J. W., 1981, *Numerical simulations using particles*, McGraw-Hill, New York

Holtzman, J., 1989, ApJS, 71, 1

Hu, W., & Sugiyama, N. 1996, ApJ, 471, 542

Hudson, M. J., Dekel, A., Courteau, S., Faber, S. M., & Willlick, J. A., 1995, MNRAS, 274, 305

Jain, B., Mo, H. J., & White, S. D. M., 1995, MNRAS, 276, L25

Kaiser, N., 1987, MNRAS, 227, 1

Kates, R. E., Kotok, E. V., & Klypin, A., 1991, A&A, 243, 295

Kauffmann, G., Nusser, A., & Steinmetz, M. 1995, preprint astro-ph/9512009

Klypin, A., Holtzman, J., Primack, J., & Regos, E., 1993, ApJ, 416, 1

Klypin, A., Primack, J.R., & Holtzman, J. 1996, ApJ, 466, 1 (KPH96)

Liddle, A. R., Lyth, D. H., Schaefer, R. K., Shafi, Q., & Viana, P. T. P., 1996a, MNRAS, 281, 531

Liddle, A. R., Lyth, D. H., Viana, P. T. P., & White, M., 1996b, MNRAS, 282, 281

Lahav, O., Lilje, P., Primack, J.R., & Rees, M. 1991, MNRAS, 251, 128

Loveday, J., Efstathiou, G., Peterson, B. A., & Maddox, S. J., 1992, ApJ, 400, L43

Ma, C. P., 1996, ApJ, 471, 13

Mo, H. J., Peacock, J. A., & Xia, X. Y., 1993, MNRAS, 260, 121

Peacock, J. A., 1992, in V. Martinez, M. Portilla, & D. Saez (eds.), *New insights into the Universe*, Proc. Valencia summer school, (Springer, Berlin), p. 1

Peacock, J. A. 1996, preprint astro-ph/9608151

Peacock, J. A., & Dodds, S. J., 1994, MNRAS, 267, 1020 (PD94)

Peacock, J. A., & Dodds, S. J., 1996, MNRAS, 280, L19 (PD96)

Peacock, J. A., & Nicholson, D., 1991, MNRAS, 253, 307

Peacock, J. A. & West, M. J., 1992, MNRAS, 259, 494

Peebles, P. J. E., 1980, *The Large-Scale Structure of the Universe* (Princeton Univ. Press, Princeton, NJ)

Primack, J.R., Holtzman, J., Klypin, A., & Caldwell, D.O. 1995, Phys. Rev. Lett., 74, 2160

Smith, C., 1995, *Master's thesis*, New Mexico State University

Sugiyama, N., 1995, ApJS 100, 281

Vogeley, M. S., Park, C., Geller, M. J., & Huchra, J. P., 1992, ApJ, 391, L5

Yepes, G., Kates, R., Khokhlov, A., & Klypin, A. 1997, MNRAS, 284, 235